Fluid flow and mass transport properties in geological disposal of high-level radioactive waste considering fracture networks

MA Guowei, *XU Man*, *CHEN Yun*, *LI Tuo*, *WANG Huidong*

(School of Civil and Transportation Engineering, Hebei University of Technology, Tianjin 300401, P. R. China)

Abstract: Fractures significantly influence fluid flow and mass transport in projects of radioactive waste disposal in deep geological formations. This work investigated the mechanism of nuclide migration in fractured rocks by considering fracture roughness based on a unified pipe-network method (UPM). The processes of adsorption and decay were incorporated into the UPM framework to capture the nuclide migration in a rock mass with rough-walled fracture networks. Benchmark tests were attempted against analytical results of the concentration distribution along a single fracture. An equivalent method to approach the hydraulic fracture aperture in fractured rocks by considering fracture roughness was also demonstrated. The influences of the fracture-roughness distribution, the rock matrix adsorption capacity and the transport properties on the process of nuclide migration were investigated. The results show that the breakthrough curve for the nuclide migration moved toward a longer time with increasing fracture roughness. The increased diffusion coefficient and retardation factor in the rock matrix greatly enhanced the matrix retardation effect on nuclide migration. Furthermore, the nuclide featured longer half-life results in a higher relative nuclide concentration of the domain. A hydraulic gradient with a relatively low value greatly impacted the relative concentration's distribution.

Keywords: high-level radioactive waste; fracture roughness; adsorption; decay; fracture networks

高放废物贮存复杂裂隙岩体的渗流传质特性

马国伟,徐曼,陈昀,李拓,王惠栋

(河北工业大学 土木与交通学院,天津 300401)

摘　要: 裂隙对高放废物深地质处置工程的渗流与传质过程影响显著。基于统一管网法(UPM),考虑裂隙网络粗糙特性及吸附与衰变因素,研究裂隙岩体核素迁移机制,并针对单裂缝岩体溶质运移解析解进行基准测试。基于粗糙裂隙网络水力隙宽等效方法,研究裂隙粗糙度分布、岩石基质吸附能力及裂隙岩体传质特性对核素迁移过程的影响。结果表明,核素运移的突破曲线随着裂隙粗糙度的增大而向长时间方向移动;岩石基质扩散系数和延迟因子的增大极大提高了其对核素迁移的延迟效应;具有较长半衰期的核素易在岩体中积聚成相对较高的浓度,而较低的水力梯度

1　Introduction

As a clean energy source, nuclear energy provides an excellent way for optimizing the energy structure and promoting sustainable development. However, the high-level radioactive waste that is produced by nuclear energy generation is one of the main factors that restrict the nuclear industry′s development. In projects of radioactive waste disposal in deep geological formations, the natural fracture network is a remarkable feature and has complex geometries and properties. Furthermore, numerous fractures with varying sizes are also created in the rock surrounding the disposal repository because of excavation blasting or earthquakes[1-3]. Since the permeability of fracture is larger than that of the rock mass matrix, fractures play a key role in fluid flow and nuclide migration (deep underground) and threaten the safe disposal of radioactive waste.

An idealized single-fracture model is commonly used to study the mechanism of fluid flow and mass transport in fractured porous media. A cubic law was derived by regarding the single fracture as two smooth, straight, and infinite parallel plates. On this basis, the fluid flow and mass transport in both single fractures and in fracture networks were analyzed[4-7]. However, natural fractures feature rough-walled properties with varying apertures and complex geometries. The assumption of parallel plates ignores the fracture roughness and the tortuous flow path, thereby overestimating the fracture′s velocity, which are not valid for fluid flow in a more realistic fracture[8-11]. Rasouli et al. [12]established a relationship between hydraulic aperture and mechanical aperture by incorporating the joint roughness coefficient (JRC) of rough-walled fractures. The applicability of the correlation was suggested by comparison to the fluid-flow test results of nine actual fractures in granite rocks. Zhang et al. [10] improved the seepage model in a single rough-walled fracture by considering the parameters of tortuosity and the joint roughness coefficient. The reliability of the updated flow prediction model, compared with the previous modified model that only considered one factor, was demonstrated by evaluating the flow patterns in four rough-walled fractures. In addition to JRC, the parameter Z_2 and fractal dimension D were also commonly used to quantitatively evaluate the fracture roughness. Li et al.[13] directly solved the Navier-Stokes equation to simulate fluid flow in a series of two-dimensional fracture models with a different fracture roughness (Z_2 is from 0 to 0.5). It was found that the hydraulic aperture was inversely proportional to Z_2. Dimadis et al. [14] proposed a correction model for the hydraulic aperture related to Z_2. The feasibility of this model was demonstrated by comparing flow velocities obtained from seepage tests. Luo et al. [15]established an equivalent permeability model using fractal dimensions to evaluate the influence of fracture roughness on the flow patterns. The fracture permeability measured by the seepage test proved the accuracy of the proposed model, which was then used in the study of coalbed methane storage and transportation.

Nuclide migration is an extremely complex process involving: convection of solute along fractures and diffusion in the matrix, mechanical dispersion of solute in fractures, adsorption by the matrix, and radioactive decay of nuclides[16]. Numerous efforts have been devoted to finding corresponding analytical solutions to investigate the mechanisms of these complex processes[17-20]. However, although analytical solutions have high accuracy, they are difficult to apply when solving complex practical problems, because they use oversimplified models. Numerical methods are powerful tools for approaching fluid flow and mass transport in rock masses with complex fracture networks. Continuum-based models can be applied

to investigate the multi-physical coupled process in fractured rocks. Tsang et al.[21] used a single-porosity model to represent fractured porous media as a single random continuum and simulated the three-dimensional transmission of point tracers at hundreds of locations in the medium. The resultant statistical distributions of transport parameters quantified the uncertainty in predicting flow and mass transport based on a limited amount of field data. A dual-porosity model indicated that the fractured rock mass was a unit composed of a fracture system with poor porosity and strong water conductivity, a pore system with good porosity and weak water conductivity. Suresh et al.[22] used the dual-porosity model to comprehensively consider the permeability of both the fracture and the rock matrix and simulated the fluid flow and mass transport in a coupled fracture-matrix system. The effects of matrix diffusion and dispersion on the concentration distribution in a typical dual-porosity system were discussed in detail. Yan et al.[23] proposed a general multiporosity model to simulate the process of seepage and mass transport in fractured rock masses with more than two porosity systems. The multiporosity model was then extended to analyze the contaminant migration behavior of porous fractured aquifers in sandstone formations[24]. It was demonstrated that a detailed description of the heterogeneous fractured aquifer was necessary to understand and simulate the distribution of pollutant concentrations.

However, continuum-based models homogenize the fracture properties, such as fracture permeability and diffusion coefficient, into the rock matrix. The discontinuity and complex geometries of the fracture are neglected, which greatly impacts the local distributions of pressure and concentration in fractured rocks[25]. Discontinuum-based models explicitly consider the distribution of fractures and their effect on the processes of fluid flow and mass transport and well describe the anisotropy of the multi-physical coupled process in a fractured rock[26]. Blessent et al.[27] employed three-dimensional and two-dimensional elements to represent the rock matrix and fractures, respectively, for the simulation of groundwater flow and pollutant transmission in fractured rocks. Verification was performed by combining the geological model and the numerical technique. Hyman et al.[28] proposed a scheme to solve the flow and mass transport in three-dimensional fracture networks. The detailed geometry of fractures was simplified, and the connected pipe networks representing the discrete fracture network (DFN) topology were retained. Sherman et al.[29] simulated the solute transport process in a fractured rock mass based on a DFN model. The particle tracking method was used to analyze the influence of different cross-mixing rules on the transport properties in a three-dimensional discrete fracture network system. Li et al.[30] used the finite element method to simulate fluid flow and solute transport in both a rock matrix and fractures. The main factors that affect the solute concentration distribution in the fracture network were investigated, and strategies for the design of radioactive waste repositories were proposed. A unified pipe-network method (UPM) was developed to investigate the coupled processes of fluid flow, mass transport, and chemical reaction in complex fracture networks[31]. The UPM was further extended to capture the mechanism of nuclide migration in highly fractured rocks by incorporating the effects of chemical convection and dispersion. The influences of the radioactive material's half-life, the fracture length and aperture, and the geometric fracture configuration on the transport of radioactive contaminants in fracture networks were numerically analyzed[32]. Fractures with complex geometries greatly impact the concentration distribution in fractured rocks, and the presence of adsorption and radioactive decay also affect nuclide migration in the formation[33]. A more comprehensive model based on UPM, therefore, must be developed to capture the mechanism of nuclide migration in fractured rocks.

The main contribution of this study was the investigation of the mechanism of nuclide migration in fractured rocks by considering fracture roughness based on the unified pipe-network method. The

processes of adsorption, decay and dispersion were incorporated into the UPM framework to capture the nuclide migration in a rock mass with rough-walled fracture networks. Firstly, mathematical models and the discrete process of UPM were introduced. Benchmark tests against analytical results of the concentration distribution along a single fracture were then attempted to verify the numerical model. An equivalent model that representing a rough-walled fracture aperture was incorporated into the UPM framework, and the influences of fracture roughness distribution, the rock matrix adsorption capacity, and the transport properties on the process of nuclide migration were investigated. Finally, conclusions were drawn, and limitations were discussed.

2 Mathematical model and numerical method

2.1 Governing equations

It is assumed that mass transport in rock fractures is mainly controlled by convection and dispersion, and the governing equation for an incompressible diluted solution is expressed as follows[31]

$$\frac{\partial(\varphi^{\xi}C^{\xi})}{\partial t}=\nabla\cdot\left(\varphi^{\xi}D^{\xi}\nabla C^{\xi}-v^{\xi}C^{\xi}\right) \quad (1)$$

where the superscript ξ is the medium type (i.e., $\xi=m$ is rock matrix, $\xi=f$ is fracture); φ is the porosity; C is the solute concentration, mol/L; v is the fluid velocity, m/s; D is the hydrodynamic dispersion coefficient, m²/s; and t is the time variable, s. The left side of the equation is the time-varying term. The first term on the right side of the equation is the dispersion term, representing the molecular diffusion and mechanical dispersion in the process of mass transport. The second term on the right side of the equation is the convection term, which is related to the fluid flow velocity.

The migration of nuclides in a fractured rock is controlled by many physical and chemical processes. In addition to the convection and dispersion described above, the adsorption and reaction of the delayed

effect should also be incorporated to capture the process of nuclide migration. Therefore, Eq. (1) can be rewritten as[32]

$$R^{\xi}\frac{\partial(\varphi^{\xi}C^{\xi})}{\partial t}=\nabla\cdot\left(\varphi^{\xi}D^{\xi}\nabla C^{\xi}-v^{\xi}C^{\xi}\right)-\lambda R^{\xi}\varphi^{\xi}C^{\xi} \quad (2)$$

where R is the retardation factor; λ is the decay constant, 1/s. The effects of adsorption on the fracture surface and the rock matrix are represented by retardation factors, which yields[32]

$$R^{f}=1+\frac{K^{f}}{b} \quad (3)$$

$$R^{m}=1+K^{m} \quad (4)$$

where K^{f} is the distribution coefficient of the fracture, m, defined as the mass of solute adsorbed in unit volume of rock matrix divided by solution concentration; K^{m} is the distribution coefficient in the rock matrix, defined as the mass of solute adsorbed in unit volume of rock matrix divided by solution concentration[34]; b is half of the fracture aperture. The relationship between the decay constant λ and the half-life $t_{1/2}$ is written as[35]

$$\lambda=\frac{\ln 2}{t_{1/2}} \quad (5)$$

2.2 Unified pipe-network method

Comparing with the finite element method (FEM), the unified pipe-network method had merit in satisfying the mass conservation by obtaining the pressure and concentration field, achieving numerical stability and convergence in the condition with a large Péclet number. Therefore, this method was used in this work to investigate the mechanism of nuclide migration in fractured rocks. In UPM, fractures and the rock matrix in a fractured model were discretized as triangular elements and line elements, respectively. A pipe-equivalent method was used to obtain the pipes for the process of fluid flow and mass transport in each element. Both fracture pipes and rock matrix pipes were then combined to generate a pipe network system[32]. A two-dimensional fractured rock is shown in Fig. 1(a). The bold red line represented a fracture, and the remainder was the rock matrix. Fig. 1(b) shows a triangular element abc of the rock matrix obtained

from the fractured model in Fig. 1(a). The point o was the circumcentre of $\triangle abc$; oi, oj and ok were the vertical lines from the circumcenter to each side of the triangle. Based on pipe equivalence, ab, bc, and ac were equivalent to matrix pipes. Specifically, the process of fluid flow between region $oibj$ and region $ojck$ was equivalent to the flow in matrix pipe bc, and the flow rate was recorded as Q_{oj}. Similarly, the flow between region $ojck$ and region $okai$ were equivalent to the fluid flow in matrix pipe ca, and the flow between region $okai$ and region $oibj$ was equivalent to the fluid flow in matrix pipe ab. Fig. 1(c) shows a fracture pipe bc, and the flow rate in the pipe was Q_{bc}. The matrix pipe and the fracture pipe were combined, based on the superposition principle, and thus, the total flow rate at the fracture-matrix interface could be obtained as $Q_{oj}+Q_{bc}$, as shown in Fig. 1(d). The process of fluid flow and mass transport was finally solved using an implicit time scheme. A detailed derivation of the discrete form based on UPM can be found in references [31-32].
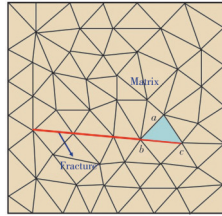
（a）A discretized model for a fractured rock
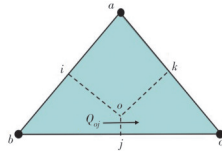
（b）Pipe equivalence in matrix element

（c）Pipe equivalence in fracture element
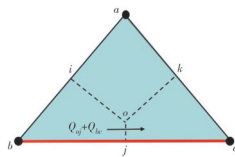
（d）Combination of matrix pipe and fracture pipe

Fig. 1　Discretization of unified pipe-network method

3　Fluid flow and mass transport in a single-fractured rock

3. 1　Model verification

A fractured rock model embedded with a horizontal fracture is shown in Fig. 2. The fractured model with dimensions of 5 m (x) × 2 m (y) was meshed with 1 918 elements and 1 015 nodes.
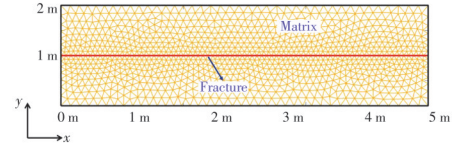
Fig. 2　Mesh generation for a fractured rock model

The upper and lower boundaries of the area were impervious. The solute was injected into the fracture at a constant concentration from the left side, and the fluid freely flowed out at the right end. The velocity of fluid in the fracture was 0.01 m/d. The initial boundary was expressed as $C(x, 0) = 0$. The simulation parameters for the process of fluid flow and mass transport are shown in Table 1.

Table 1　Simulation parameters for model verification

Parameters	Symbols	Values	Units
Fluid density	ρ^{f}	1 000	kg/m^3
Fracture aperture	b	1×10^{-3}	m
Fracture porosity	φ^{f}	1	
Matrix porosity	φ^{m}	0. 2	
Matrix permeability	k^{m}	1×10^{-15}	m^2
Fracture diffusion coefficient	D^{f}	$5. 9 \times 10^{-8}$	m^2/s
Matrix diffusion coefficient	D^{m}	$1. 6 \times 10^{-10}$	m^2/s
Retardation coefficient in matrix	R^{m}	1. 27	
Retardation coefficient in fracture	R^{f}	1. 5	
Decay constant of nuclide	λ	$1. 78 \times 10^{-9}$	s^{-1}

The numerical model was verified by comparison with the analytical solution for the concentration evolution in a single fracture with constant aperture. In a single-fractured model that considers the processes of convection and diffusion, the analytical solution of mass transport in the fracture can be expressed as[18]

$$\frac{C}{C_0} = \mathrm{erfc}\left\{\left(\frac{t_{\mathrm{w}}}{b} \cdot \frac{D_{\mathrm{e}}}{\sqrt{D_{\mathrm{a}}}}\right) \bigg/ \left[2\sqrt{(t - t_{\mathrm{w}})}\right]\right\} \quad (6)$$

where c_0 is the source comcentration at the inlet, mol/L; t_w is the water residence time, s; t is the solute transport time, s; D_e is the effective diffusion coefficient, m²/s, and D_a is the apparent diffusion coefficient, m²/s.

The relative concentration distribution curves along the single fracture at different times (200, 2 000 and 10 000 d) are displayed in Fig. 3. The concentration in the fracture was negatively correlated with the migration distance, and the concentration at the same position increased with increasing simulation time. Good agreement was achieved between the results obtained from the UPM and the analytical solutions.
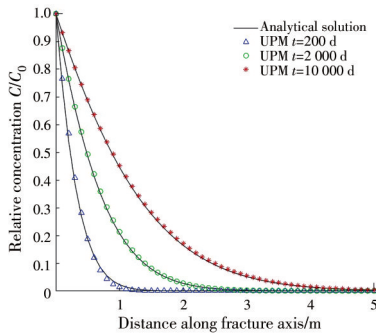
Fig. 3　Comparison of analytical and numerical solutions for the processes of convection and diffusion in a single-fractured model

If the adsorption and reaction of the delayed effect are incorporated in the process of mass transport, the analytical solution can be expressed as[17]

$$\frac{C}{C_0} = \exp\left\{ \left[v - \left(v^2 + \frac{\psi}{D^f} \right)^{1/2} \right] \cdot x \right\} \qquad (7)$$

Fig. 4 shows the relative concentration distribution curves along the single fracture at 200, 2 000 and 10 000 d. The concentration of nuclides in the fracture decreased with increasing migration distance. The nuclide migration speed, considering the effect of adsorption and decay, significantly decreased. The results obtained from the numerical model were consistent with the analytical solutions, which indicated the reliability of the UPM in the simulation of chemical convection, diffusion, adsorption and decay in a fractured model.
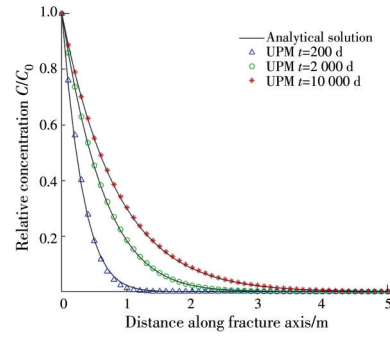
Fig. 4　Comparison of analytical and numerical solutions considering the processes of convection, diffusion, adsorption and decay in a single-fractured model

3.2　Fracture roughness characterization and equivalent hydraulic aperture

The joint roughness coefficient (JRC), fractal dimension (D), and parameter Z_2 are widely used in rock mechanics to quantitatively evaluate fracture roughness. The parameter Z_2, which is conceptually clear and computationally simple, represents the fracture roughness in a two-dimensional rock mass in this study[36].

$$z_2 = \left[\frac{1}{L} \sum \left(\frac{z_{i-1} - z_i}{x_{i-1} - x_i} \right)^2 (x_{i-1} - x_i) \right]^{1/2} \qquad (8)$$

where x_i and z_i are the coordinates of the fracture surface profile, m; L is the fracture length, m. The correlations between JRC and Z_2 can be found based on the analysis of Barton's standard profile curve[37].

Mathematical and empirical models have been proposed to connect hydraulic apertures with mechanical apertures[12-13, 38-39]. The established correlation between these apertures and Z_2 is employed[40].

$$e = \frac{E}{1 + Z_2^{2.25}} \qquad (9)$$

where e is the hydraulic aperture, m; E is the mechanical aperture, m. The above correlation is applicable to fluid flow with a Reynolds number less than 1.

SynFrac[41-42] was used to generate the rough-walled fracture embedded in a rock mass, as shown in Fig. 5. The fracture aperture followed a normal distribution with a mean value of 0.1 mm. The parameter Z_2 of this rough-walled fracture was 0.3, as obtained from Eq. (8). Thus, the equivalent hydraulic aperture could be calculated as 0.094 mm

by substituting Eq. (8) into Eq. (9).
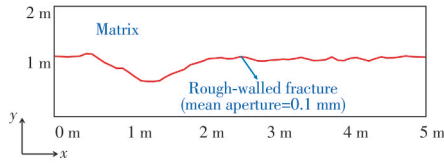
Fig. 5 A rough-walled fracture generated based on SynFrac

3.3 Transport properties in a single-fractured model

A rough-walled fracture with parameter Z_2 of 0.3 and an average aperture of 0.1 mm was generated in a two-dimensional fractured model. A smooth-walled fracture with an equivalent hydraulic aperture of 0.094 mm was then obtained based on Eq. (9). The simulation parameters and boundary conditions can be found in Section 3.1. The simulated results indicated that the average flow rate in a rough-walled fracture was 3.46×10^{-13} m³/s, while the average flow rate in a smooth-walled fracture was 4.60×10^{-13} m³/s. The flow rate in a rough-walled fracture was 24.8% less than that in a smooth-walled fracture.

Breakthrough curves and relative concentration distribution curves were obtained and plotted in Fig. 6. As shown in Fig. 6(a), the increase rate of nuclide concentration in the smooth-walled fracture was obviously faster than that of the rough-walled fracture. As shown in Fig. 6(b), it was indicated that the migration distance required for the smooth-walled fracture to reach the same relative concentration was longer than that required for the rough-walled fracture. Table 2 lists the time required to reach the identical relative concentration at outlets for the two models with different types of fractures. It was illustrated that 500 d was required for the smooth-walled fracture model to reach a relative concentration of 0.05, which was 1 600 d earlier than that for the rough-walled fracture model. The time difference between these two models to reach relative concentrations of 0.1 and 0.15 at the outlets was 2 800 d and 5 400 d, respectively, which indicated that the impact of fracture roughness was enhanced as the migration process continued. Therefore, the effect of fracture roughness should be considered in the investigation of nuclide migration in fractured rocks.
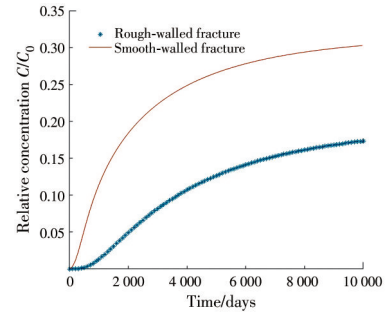
(a) Breakthrough curves
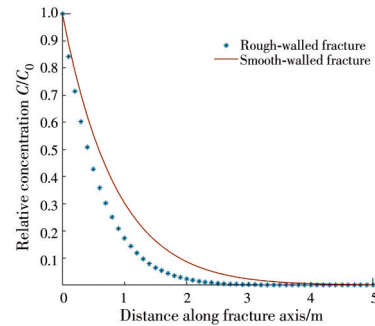
(b) The relative concentration along the x-direction after 10 000 days

Fig. 6 The evolution of relative nuclide concentration in a fractured rock with different fracture properties

Table 2 The time required for a single-fractured model to reach different relative concentrations

Fracture type	Time/days		
	0.05 C_0	0.1 C_0	0.15 C_0
Rough-walled fracture	2 100	3 700	6 800
Smooth-walled fracture	500	900	1 400

4 Transportation of high-level radioactive waste in rough-walled fracture networks

4.1 Description of the model

Two groups of fractures were randomly generated in the region of 50 m (x) × 50 m (y). The fracture dip angle in each group followed a normal distribution with mean values of 45° and 135°, respectively, and the variance was 5. The fracture length followed a normal distribution with an average value of 10 m and a variance of 6. The fracture aperture conformed to the normal distribution with an average value of 0.5 mm in the study of

radioactive waste's deep geological disposal in fractured rocks. The total fracture number was 100 in the current simulation, and the model diagram is shown in Fig. 7.
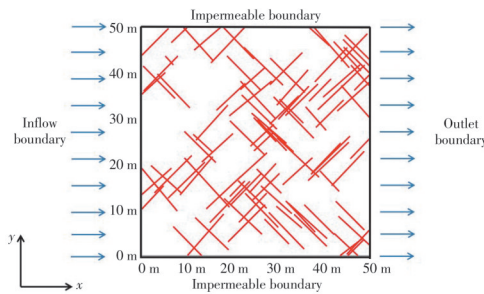
Fig. 7   A rock model with fractured networks for nuclide migration

The hydraulic gradient was commonly distributed in the range of 0.008-0.016 based on previous investigations[43]. The hydraulic gradient was assigned as $J=0.01$ in the current simulation. The fluid at the right end of the area freely flowed out, and the upper and lower parts were impermeable boundaries, as shown in Fig. 7. The solute was injected at a constant concentration along the x-direction from the left boundary and flowed out at $x=50$ m. Here, the nuclide Th-232 was employed to simulate a migration process in the fractured system. The simulation parameters are listed in Table 3.

Table 3   Simulation parameters for the fluid flow and mass transport in fracture network

Parameters	Symbols	Values	Units
Fluid density	ρ^f	1 000	kg/m³
Average fracture aperture	E	0.5	mm
Fracture porosity	φ^f	1	
Matrix porosity	φ^m	0.2	
Matrix permeability	K^m	1×10^{-15}	m²
Fracture diffusion coefficient	D^f	8×10^{-5}	m²/s
Matrix diffusion coefficient	D^m	1.6×10^{-10}	m²/s
Retardation coefficient in matrix	R^m	1.27	
Retardation coefficient in fracture	R^f	1.5	
Decay constant of nuclide	λ	4.93×10^{-11}	a⁻¹

4.2   Effect of fracture roughness distributions on nuclide migration

The fracture roughness is determined by the aperture and tortuosity of a fracture. The process of

nuclide migration in fracture networks with different roughness distributions was studied in this section. Each fracture in the fracture network system featured a specific fracture roughness. Cases with different distributions of fracture roughness (constant roughness, uniform distribution of roughness and normal distribution of roughness) were numerically simulated to investigate the effect of fracture roughness on the process of nuclide migration in rough-walled fracture networks. Two values of Z_2 ($Z_2=0$ and $Z_2=0.5$) were assigned in cases with constant roughness. The fracture roughness in cases of uniform distribution and normal distribution were in the range of 0 and 0.5. An average value of 0.25 and a variance of 0.1 was assigned in the normal distribution case.

Breakthrough curves for the nuclide concentration along the exit of the domain in different cases related to fracture roughness are shown in Fig. 8. The breakthrough curve moved towards a longer time with increasing Z_2. The concentration at the outlet boundary decreased with increasing overall roughness. The breakthrough curve of the roughness uniform distribution model was close to that of the normal distribution model.
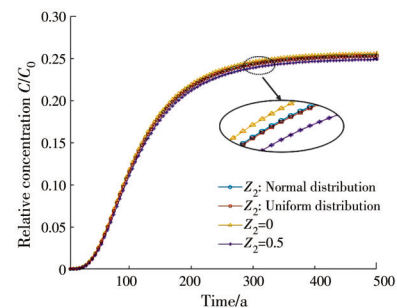
Fig. 8   Comparison of breakthrough curves of different distributions of roughness

4.3   Effect of rock matrix properties on nuclide migration

The water storage capacity of a fractured rock mass depends on microcracks or pores (rock matrix), while the water conductivity depends on larger fractures. Therefore, both fractures and the rock matrix were considered in the simulation of nuclide migration in fractured rocks. Two aspects related to the influence of the rock matrix on the processes of fluid flow and mass transport were investigated. The

first was the diffusion coefficient of the matrix (D^m), and the second was the blocking factor of the matrix (R^m) when nuclides were adsorbed.

　　The influence of matrix diffusion on the process of nuclide migration in a fractured system was analyzed using four different diffusion coefficients: 0, 1.6×10^{-12}, 1.6×10^{-11} and 1.6×10^{-10} m²/s. The breakthrough curves for different cases are plotted in Fig. 9. The average concentration of nuclides in the fractures at the outlet boundary tended to be stable after 300 a, and it decreased with increasing D^m. Fig. 10 presents the distribution of nuclide concentration with different matrix diffusion coefficients. The concentration distribution at the outlet boundary indicated that the concentration of nuclides in the fractures decreased with increasing D^m. It has been demonstrated that enhanced matrix diffusion greatly slowed the process of nuclide migration and weakened the peak value of the breakthrough curve.

Fig. 9　Comparison of breakthrough curves of different D^m

(a) $D^m = 0$　　　　　(b) $D^m = 1.6 \times 10^{-12}$

(c) $D^m = 1.6 \times 10^{-11}$　　　　　(d) $D^m = 1.6 \times 10^{-10}$
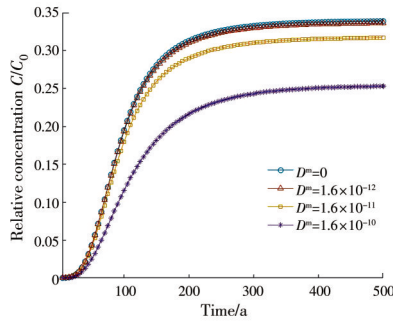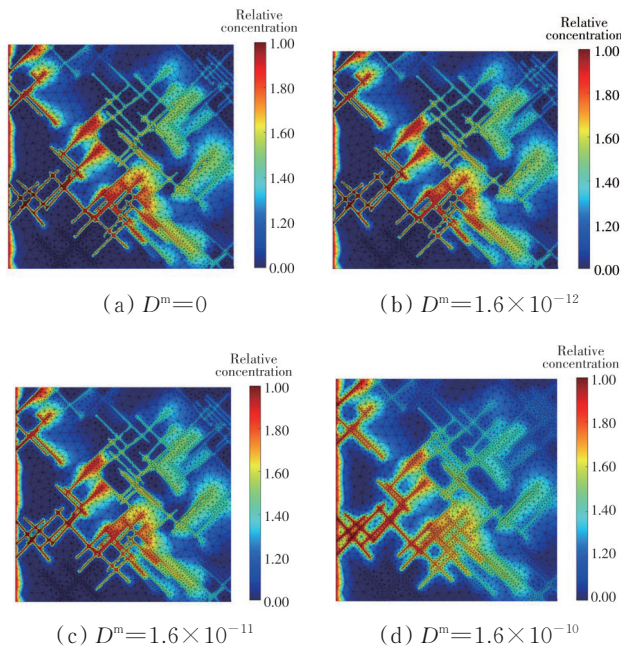
Fig. 10　Distribution of nuclide in fracture network

Different R^m values were used to analyze the effect of adsorption on the processes of nuclide migration in fractured rocks, and the breakthrough curves are shown in Fig. 11. The relative concentration of nuclides at the outlet decreased with increasing R^m. The enhanced adsorption effect in the rock matrix extended the breakthrough time as the nuclide continuously migrated in the domain.
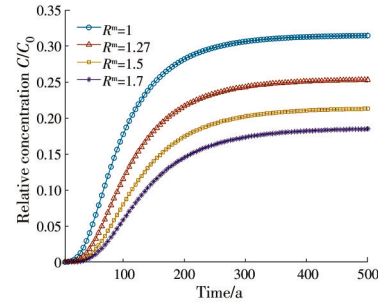
Fig. 11　Comparison of breakthrough curves of different R^m

4.4　Effects of decay on nuclide migration

　　The radioactive decay of nuclides also impacted the mass transport process in the domain. Nuclides, including Th-232, U-238 and Cs-135, which have large differences in half-lives (Table 4), were used to characterize the nuclide migration in fractured rocks. Fig. 12 illustrates the distribution of nuclide concentrations after 50 a. Th-232 diffused the fastest in the same domain compared with the other two nuclides.

Table 4　The half-lives and decay constants of different nuclides

Nuclide	Half-life $t_{1/2}$/a	Decay constant λ/a^{-1}
Th-232	1.41×10^{10}	4.93×10^{-11}
U-238	4.50×10^{9}	1.54×10^{-10}
Cs-135	2.30×10^{6}	3.01×10^{-7}

　　The relative concentrations of the three nuclides at the outlet of the fractured rock were calculated. The corresponding breakthrough curves and the relative concentrations along the x-direction are shown in Fig. 13.

　　The breakthrough curves in Fig. 13(a) indicated that the relative concentrations of all nuclides at the outlet boundary increase with time. The nuclide Cs-135, which has a shorter half-life, featured the lowest relative

（a）Th-232　　　　　　（b）U-238

（c）Cs-135
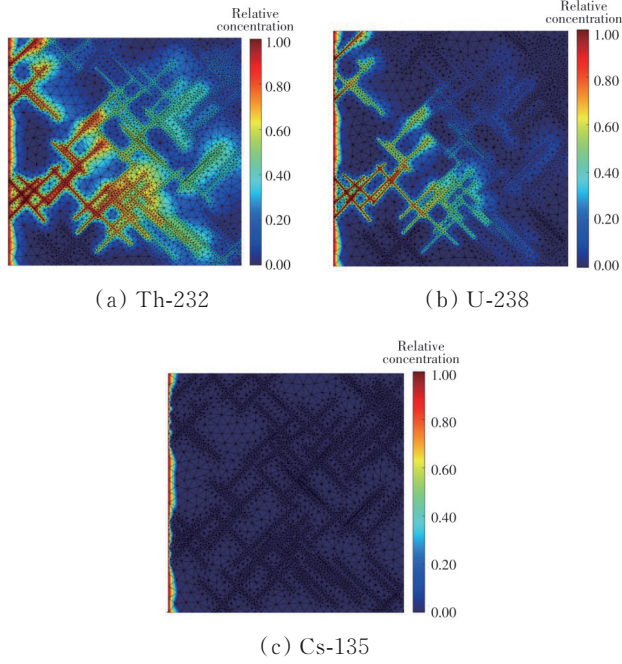
Fig. 12　Distribution of the concentration of different nuclides in a fractured rock

（a）Breakthrough curves

（b）The relative concentration along the x-direction after 50 a
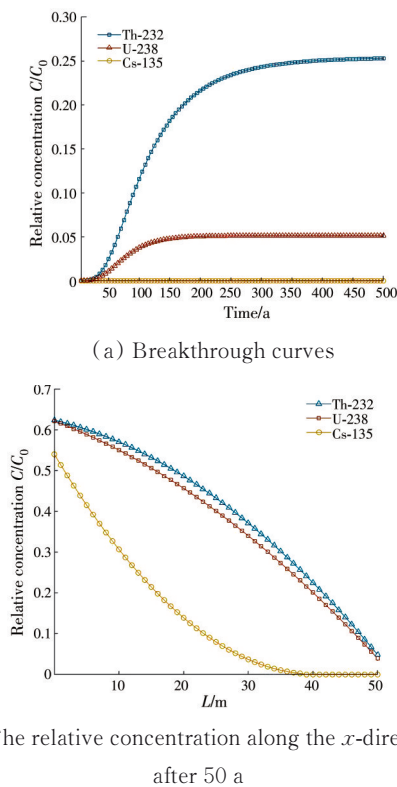
Fig. 13　The evolution of relative nuclide concentrations of different nuclides

concentration at the outlet compared with the other two nuclides. The concentration built up at an exponential rate before 100 a and tended to be stable after 200 a.

The time required to reach a stable state was longer for nuclides with longer half-life. Fig. 13(b) illustrates the relative concentrations of three nuclides migrating along the x-direction in the fractured domain after 50 a. The relative concentration in fractures decreased with increasing migration distance. The nuclide Cs-135 was characterized by a smaller half-life and presented a smaller migration distance. Correspondingly, the nuclide Th-232 had a longer half-life and tended to have a lower radiation intensity and a longer migration distance. The decay of a radionuclide emitted and transformed particles into other elements. A more active radiation reaction resulted in a faster decrease in the nuclide concentration and shorter penetration distance[44]. Therefore, the nuclide's radioactive decay strongly impacted the distribution of the nuclide concentration in fractured rocks.

4.5　Effects of hydraulic gradient on nuclide migration

Different hydraulic gradients (0.008, 0.01, 0.012 and 0.015) were used to investigate nuclide migration in the fractured domain. The distributions of nuclide concentration after 50 a in the four cases are shown in Fig. 14.

The breakthrough curves in Fig. 15 (a)

（a）J=0.008　　　　　　（b）J=0.010

（c）J=0.012　　　　　　（d）J=0.015
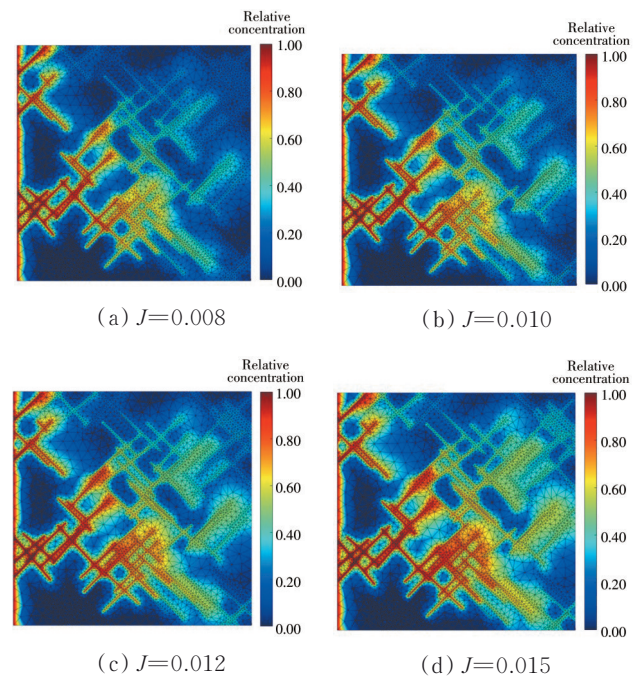
Fig. 14　Distribution of nuclide concentration in different hydraulic gradients

indicated that the relative concentration at the outlet increased with increasing hydraulic gradient throughout the simulation. In addition, the relative concentration increased by 30.4% when the hydraulic gradient changed from 0.008 to 0.01 (increased by 25%). Nevertheless, the relative concentration only increased by 22.0% when the hydraulic gradient changed from 0.012 to 0.015 (increased by 25%). The results indicated that the concentration variation was greatly influenced by the hydraulic gradient when J was a relatively low value. Fig. 15(b) shows the relative concentration along the x-axis after 50 a with different hydraulic gradients. The maximum migration distance of the nuclide increased with increasing hydraulic gradient.
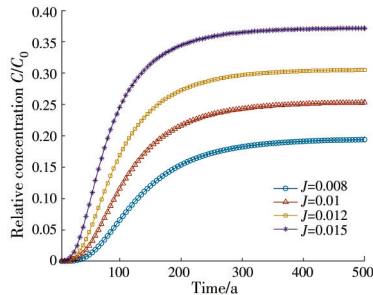
（a）Breakthrough curves
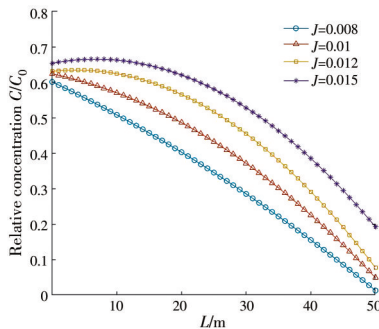
（b）The relative concentration along the x-direction

after 50 a

Fig. 15　The evolution of relative nuclide concentration considering different hydraulic gradients

5　Conclusion

This work was used to investigate the mechanism of nuclide migration in fractured rocks when considering fracture roughness based on UPM. The influences of the fracture roughness' distribution, the nuclide decay effect, the rock matrix adsorption capacity and the transport properties on the process of nuclide migration were investigated. The results showed that different distributions of roughness had an effect on the nuclide concentration in fractured rock and that the breakthrough curve moved toward a longer time with increasing Z_2. However, the migration patterns between the case with the uniform distribution of Z_2 were close to the case with the normal distribution of Z_2. The increase of D^m and R^m in the rock matrix greatly enhanced the matrix retardation effect on nuclide migration. The half-life of the nuclide also greatly influenced the distribution of nuclide concentration in the fractured rock. A longer nuclide half-life led to a higher level of relative nuclide concentration in the domain. Furthermore, the hydraulic gradient greatly impacted the distribution of the relative concentration, especially when the hydraulic gradient was relatively low. The relative concentration increased by 30.4% when the hydraulic gradient changed from 0.008 to 0.01 (increased by 25%). Nevertheless, the relative concentration only increased by 22.0% when the hydraulic gradient changed from 0.012 to 0.015 (increased by 25%).

The current numerical model provided a theoretical basis for the optimization of high-level radioactive waste disposal in fractured rocks. However, improvements are still required in future work. A more realistic geological model should be established to perform safety assessments in the deep geological disposal of high-level radioactive waste based on field data. Furthermore, the influences of temperature and fracture filling on the process of nuclide migration should also be considered.

References

[1] WANG X, QIN Y, YIN Z H, et al. Historical shear deformation of rock fractures derived from digital outcrop models and its implications on the development of fracture systems [J]. International Journal of Rock Mechanics and Mining Sciences, 2019, 114: 122-130.

[2] FAN L F, GAO J W, DU X L, et al. Spatial gradient distributions of thermal shock-induced damage to granite [J]. Journal of Rock Mechanics and Geotechnical

Engineering, 2020, 12(5): 917-926.

[3] FAN L F, YANG K C, WANG M, et al. Experimental study on wave propagation through granite after high-temperature treatment [J]. International Journal of Rock Mechanics and Mining Sciences, 2021, 148: 104946.

[4] SISAVATH S, AL-YAARUBY A, PAIN C C, et al. A simple model for deviations from the cubic law for a fracture undergoing dilation or closure [J]. Pure and Applied Geophysics, 2003, 160(5/6): 1009-1022.

[5] KONZUK J S, KUEPER B H. Evaluation of cubic law based models describing single-phase flow through a rough-walled fracture [J]. Water Resources Research, 2004, 40(2): W02402.

[6] BODIN J, POREL G, DELAY F, et al. Simulation and analysis of solute transport in 2D fracture/pipe networks: The SOLFRAC program [J]. Journal of Contaminant Hydrology, 2007, 89(1/2): 1-28.

[7] PENG H, ZHAO Z H, CHEN W, et al. Thermal effect on permeability in a single granite fracture: Experiment and theoretical model [J]. International Journal of Rock Mechanics and Mining Sciences, 2020, 131: 104358.

[8] BRIGGS S, KARNEY B W, SLEEP B E. Numerical modelling of flow and transport in rough fractures [J]. Journal of Rock Mechanics and Geotechnical Engineering, 2014, 6(6): 535-545.

[9] WANG L C, CARDENAS M B, SLOTTKE D T, et al. Modification of the local cubic law of fracture flow for weak inertia, tortuosity, and roughness [J]. Water Resources Research, 2015, 51(4): 2064-2080.

[10] ZHANG G, TIAN Y, LI Y J. Numerical study on the mechanism of fluid flow through single rough fractures with different JRC [J]. Scientia Sinica Physica, Mechanica & Astronomica, 2019, 49(1): 014701.

[11] CRANDALL D, BROMHAL G, KARPYN Z T. Numerical simulations examining the relationship between wall-roughness and fluid flow in rock fractures [J]. International Journal of Rock Mechanics and Mining Sciences, 2010, 47(5): 784-796.

[12] RASOULI V, HOSSEINIAN A. Correlations developed for estimation of hydraulic parameters of rough fractures through the simulation of JRC flow channels [J]. Rock Mechanics and Rock Engineering, 2011, 44(4): 447-461.

[13] LI B, JIANG Y J. Quantitative estimation of fluid flow mechanism in rock fracture taking into account the influences of JRC and Reynolds number [J]. Journal of the Mining and Materials Processing Institute of Japan,

2013, 129(7): 479-484.

[14] DIMADIS G, DIMADI A, BACASIS I. Influence of fracture roughness on aperture fracture surface and in fluid flow on coarse-grained marble, experimental results [J]. Journal of Geoscience and Environment Protection, 2014, 2(5): 59-67.

[15] LUO Y F, XIA B W, LI H L, et al. Fractal permeability model for dual-porosity media embedded with natural tortuous fractures [J]. Fuel, 2021, 295: 120610.

[16] DING X H, FENG S J, ZHENG Q T, et al. A two-dimensional analytical model for organic contaminants transport in a transition layer-cutoff wall-aquifer system [J]. Computers and Geotechnics, 2020, 128: 103816.

[17] TANG D H, FRIND E O, SUDICKY E A. Contaminant transport in fractured porous media: Analytical solution for a single fracture [J]. Water Resources Research, 1981, 17(3): 555-564.

[18] ZHAO Z H, JING L R, NERETNIEKS I, et al. Analytical solution of coupled stress-flow-transport processes in a single rock fracture [J]. Computers & Geosciences, 2011, 37(9): 1437-1449.

[19] ZHU Y H, ZHAN H B, JIN M G. Analytical solutions of solute transport in a fracture-matrix system with different reaction rates for fracture and matrix [J]. Journal of Hydrology, 2016, 539: 447-456.

[20] OGATA S, YASUHARA H, KINOSHITA N, et al. Modeling of coupled thermal-hydraulic-mechanical-chemical processes for predicting the evolution in permeability and reactive transport behavior within single rock fractures [J]. International Journal of Rock Mechanics and Mining Sciences, 2018, 107: 271-281.

[21] TSANG Y W, TSANG C F, HALE F V, et al. Tracer transport in a stochastic continuum model of fractured media [J]. Water Resources Research, 1996, 32(10): 3077-3092.

[22] SURESH KUMAR G. Mathematical modeling of groundwater flow and solute transport in saturated fractured rock using a dual-porosity approach [J]. Journal of Hydrologic Engineering, 2014, 19(12): 04014033.

[23] YAN B C, ALFI M, AN C, et al. General Multi-Porosity simulation for fractured reservoir modeling [J]. Journal of Natural Gas Science and Engineering, 2016, 33: 777-791.

[24] LAGENDIJK V R, VOGEL T, KÖNGETER J. Contaminant transport modeling in multi-porosity fractured systems using a multi-continuum approach [M]//Geoecology and Computers. London; New York : Routledge, 2018: 497-502.

[25] MA G W, WANG Y, LI T, et al. A mesh mapping method for simulating stress-dependent permeability of three-dimensional discrete fracture networks in rocks [J]. Computers and Geotechnics, 2019, 108: 95-106.

[26] HADGU T, KARRA S, KALININA E, et al. A comparative study of discrete fracture network and equivalent continuum models for simulating flow and transport in the far field of a hypothetical nuclear waste repository in crystalline host rock [J]. Journal of Hydrology, 2017, 553: 59-70.

[27] BLESSENT D, THERRIEN R, MACQUARRIE K. Coupling geological and numerical models to simulate groundwater flow and contaminant transport in fractured media [J]. Computers & Geosciences, 2009, 35(9): 1897-1906.

[28] HYMAN J D, KARRA S, MAKEDONSKA N, et al. dfnWorks: A discrete fracture network framework for modeling subsurface flow and transport [J]. Computers & Geosciences, 2015, 84: 10-19.

[29] SHERMAN T, HYMAN J D, BOLSTER D, et al. Characterizing the impact of particle behavior at fracture intersections in three-dimensional discrete fracture networks [J]. Physical Review E, 2019, 99(1): 013110.

[30] LI X X, LI D Q, XU Y, et al. A DFN based 3D numerical approach for modeling coupled groundwater flow and solute transport in fractured rock mass [J]. International Journal of Heat and Mass Transfer, 2020, 149: 119179.

[31] CHEN Y, MA G W, LI T, et al. Simulation of wormhole propagation in fractured carbonate rocks with unified pipe-network method [J]. Computers and Geotechnics, 2018, 98: 58-68.

[32] MA G W, LI T, WANG Y, et al. Numerical simulations of nuclide migration in highly fractured rock masses by the unified pipe-network method [J]. Computers and Geotechnics, 2019, 111: 261-276.

[33] CHUGUNOV V, FOMIN S. Effect of adsorption, radioactive decay and fractal structure of matrix on solute transport in fracture [J]. Philosophical Transactions Series A, Mathematical, Physical, and Engineering Sciences, 2020, 378(2172): 20190283.

[34] FREEZE R A, CHERRY J A. Groundwater [M]. Englewood Cliffs: Prentice Hall, 1979.

[35] LIESER K H. Nuclear and radiochemistry: Fundamentals and applications [M]. New Jersey: John Wiley & Sons, 2008.

[36] MYERS N O. Characterization of surface roughness [J]. Wear, 1962, 5(3): 182-189.

[37] TSE R, CRUDEN D M. Estimating joint roughness coefficients [J]. International Journal of Rock Mechanics and Mining Sciences & Geomechanics Abstracts, 1979, 16(5): 303-307.

[38] XIONG X B, LI B, JIANG Y J, et al. Experimental and numerical study of the geometrical and hydraulic characteristics of a single rock fracture during shear [J]. International Journal of Rock Mechanics and Mining Sciences, 2011, 48(8): 1292-1302.

[39] OLSON J E. Sublinear scaling of fracture aperture versus length: An exception or the rule? [J]. Journal of Geophysical Research: Solid Earth, 2003, 108(B9): 2413.

[40] ZHAO Z H, LI B, JIANG Y J. Effects of fracture surface roughness on macroscopic fluid flow and solute transport in fracture networks [J]. Rock Mechanics and Rock Engineering, 2014, 47(6): 2279-2286.

[41] BABADAGLI T, DEVELI K. Fractal characteristics of rocks fractured under tension [J]. Theoretical and Applied Fracture Mechanics, 2003, 39(1): 73-88.

[42] SCHWARZ J O, ENZMANN F. Simulation of fluid flow on fractures and implications for reactive transport simulations [J]. Transport in Porous Media, 2013, 96(3): 501-525.

[43] HIBIYA K, INABA T, SHIOGAMA Y, et al. A study on groundwater flow in Japan: JNC TN7400 99-004 [R]. Tokai, Japan: Japan Nuclear Cycle Development Insitute (JNC), 1999.

[44] GALETTI D, MIZRAHI S S. The delimiting/frontier lines of the constituents of matter [J]. arXiv, 2019: 1909.07223.

（编辑　黄廷）